BJR

Received: 29 July 2015 | Revised: 6 October 2015 | Accepted: 19 October 2015

doi: 10.1259/bjr.20150633

Cite this article as:
Feng DX, McCauley JP, Morgan–Curtis FK, Salam RA, Pennell DR, Loveless ME, et al. Evaluation of 39 medical implants at 7.0 T. *Br J Radiol* 2015; **88**: 20150633.

FULL PAPER

Evaluation of 39 medical implants at 7.0 T

[1]DAVID X FENG, [1]JOSEPH P MCCAULEY, [1]FEA K MORGAN–CURTIS, [1]REDOAN A SALAM, [2]DAVID R PENNELL, MS, [1]MARY E LOVELESS, PhD and [2,3]ADRIENNE N DULA, PhD

[1]School for Science and Math at Vanderbilt University, Vanderbilt University, Nashville, TN, USA
[2]Vanderbilt University Institute of Imaging Science, Vanderbilt University Medical Center, Nashville, TN, USA
[3]Department of Radiology and Radiological Sciences, Vanderbilt University Medical Center, Nashville, TN, USA

Address correspondence to: Dr Adrienne N Dula
E-mail: *Adrienne.N.Dula@vanderbilt.edu*

The authors David X Feng, Joseph P McCauley, Fea K Morgan–Curtis and Redoan A Salam contributed equally to this article.

Objective: With increased signal to noise ratios, 7.0-T MRI has the potential to contribute unique information regarding anatomy and pathophysiology of a disease. However, concerns for the safety of subjects with metallic medical implants have hindered advancement in this field. The purpose of the present research was to evaluate the MRI safety for 39 commonly used medical implants at 7.0 T.
Methods: Selected metallic implants were tested for magnetic field interactions, radiofrequency-induced heating and artefacts using standardized testing techniques.
Results: 5 of the 39 implants tested may be unsafe for subjects undergoing MRI at 7.0 T.
Conclusion: Implants were deemed either "MR Conditional" or "MR Unsafe" for the 7.0-T MRI environment. Further research is needed to expand the existing database categorizing implants that are acceptable for patients referred for MRI examinations at 7.0 T.
Advances in knowledge: Lack of MRI testing for common metallic medical implants limits the translational potential of 7.0-T MRI. For safety reasons, patients with metallic implants are not allowed to undergo a 7.0-T MRI scan, precluding part of the population that can benefit from the detailed resolution of ultra-high-field MRIs. This investigation provides necessary MRI testing of common medical implants at 7.0 T.

INTRODUCTION

MRI is a well-established imaging modality commonly used for diagnosis and treatment monitoring, as well as utilized as an end point in clinical trials. In theory, the observed MRI signal increases with the square of the strength of the static magnetic field. Therefore, higher field strengths translate to an increased signal to noise ratio, which can be leveraged for higher achievable resolution, better anatomical coverage or a decreased imaging time compared with lower field strengths. As a result of the differential contributions of various contrast mechanisms compared with lower field strength MRI systems, 7.0-T MRI scanners have increasingly been applied to examine clinical pathology, suggesting improvements in sensitivity as well as novel information regarding pathology *in vivo*. The clinical utility of 7.0-T imaging of the brain[1] has emerging applications in surgical planning[2] and pathologies such as epilepsy,[3,4] glioma,[5,6] multiple sclerosis,[7–9] Alzheimer's disease,[10,11] stroke[12] and Parkinson's disease.[13]

The increase in static magnetic field strength necessitates better understanding of the challenges to ensure safety of the imaging subjects and patients. Biomedical implants are commonly a contraindication for 7.0-T MRI examination owing to interactions with the static magnetic field, radiofrequency (RF) implications and the requirement for more powerful gradients associated with 7.0-T MRI scanners. Restrictions such as these preclude a large subset of patients from the known advantages at 7.0-T MRI while accentuating the need for systematic safety analyses of commonly used surgical implants in order for 7.0-T MRI to attain its potential clinical utility. Although standardized testing procedures exist to properly determine the safety implications for an implant in association with MRI scanners, to date, comprehensively testing of multiple metallic implants at 7.0 T is still in its infancy.

MRI systems use multiple magnetic fields including static magnetic fields (B_0), spatial gradient fields, time-varying magnetic fields and pulsed magnetic fields (B_1). The static magnetic field is the homogeneous magnetic field strength at the isocentre of the scanner. Within the static magnetic field, as one moves towards or away from the isocentre of MRI, the field strength changes, creating what is called the

spatial gradient magnetic field.[14] The pulsed magnetic field refers to the RF fields transmitted during an imaging sequence. This pulsed RF field produces energy that the body absorbs and disperses typically in the form of heat. The time-varying magnetic field (dB/dt) provides position-dependent variation in the magnetic field strength, which can induce electrical currents, known to cause heating. All of these fields exert unique forces upon a metallic implant in a patient undergoing MRI.

In order to ensure the safety of research participants and healthcare workers, the behaviour of metallic implants needs to be assessed in the presence of these fields. Each field interacts with the implants in a unique way, resulting in displacement, RF-related heating or even disturbances in the images produced. The spatial gradient field causes translational attractive forces to act on some metallic implants, pulling them towards the isocentre of the magnet.[15] Because ferromagnetic objects are inclined to accelerate towards the isocentre of MRI, the possibility of a translating implant must be taken into consideration, as it could cause critical injury to the patient or others in the MR suite. The static magnetic field also creates rotational displacement, or torque, on some implants resulting in alignment of the metallic implant to the static magnetic field, potentially resulting in a serious injury. The speed of alignment and force of the torque depends on the shape and composition of the implant. Differences in the susceptibility of the implant *vs* the surrounding tissue to the static magnetic field cause disruptions in the signal and produce image artefacts.[16] Image artefacts do not cause the patient physical harm but can make image analysis within the region around the implant difficult for physicians and researchers. The pulsed RF field transmits energy that is absorbed by the body that can cause heating in the implants to such a degree that when the heat disperses to the surrounding tissue, it causes damage.

It is necessary to establish and maintain a database for commonly used metallic medical implants, such as that existing for clinical field strengths (www.mrisafety.com),[17] which can be used as a guide for inclusion of volunteer subjects and patients to undergo MRI procedures using 7.0-T MRI scanners in research studies. The critical limits for relevant safety concerns related to the static, gradient and RF fields must be assessed using regulations and methods such as those provided by the American Society for Testing and Materials or the joint working group between the International Standards Organization and the International Electrotechnical Commission. Efforts are made by all standards organizations to address MRI safety and compatibility for the entire spectrum of medical devices and equipment that may be introduced into the MRI environment without duplication.[18]

The American College of Radiology, through its Subcommittee on MR Safety, has proposed a standardized terminology that will contribute to greater safety and understanding for screening metal implants and/or devices prior to MRI.[19] Through testing, implants are categorized as being "MR Safe", "MR Conditional" or "MR Unsafe" in the MRI environment.[15] "MR Conditional" describes an implant that has been demonstrated to pose no known risks in a specific MRI environment (static magnetic field strength, spatial gradient, dB/dt, and RF field) according to the ASTM standards.[19–21] This could include metallic implants and requires testing for all effects listed above, while any parameter or condition that affects the item must be listed and described. "MR Unsafe" implants are known to pose danger as a result of interactions with the magnetic field during one of the four tests listed above and are seen as unfit for the MRI environment according to the standards given by the ASTM. These implants should not be allowed into the MRI environment. All testing is unique to the specific MRI environment and implant composition, necessitating accurate labelling and cataloguing of each implant model number and composition.

Safety in 1.5- and 3.0-T MRI environments, including the testing of over 5000 medical implants, has been well characterized (www.mrisafety.com),[17] while studies[22–25] looking at the effects of a 7.0-T MRI environment on said implants have only recently occurred and few implants have been tested for safety precautions at this higher magnitude. As a result, any biomedical implant that has not been classified as "MR Safe" is currently a contraindication for 7.0-T MRI examinations, thus limiting the pool of possible candidates for important research and clinical studies. The present study provides information on the effects of the 7.0-T MRI environment on 39 common biomedical implants to continue expanding this database. The implants selected ranged from aortic stents to orthopaedic implants, as shown in Table 1, although none of the implants examined had any active mechanical functions. As further studies document the safety of more implants, the list of contraindications can be reduced to expand subject participation and support further development of this promising technology.

METHODS AND MATERIALS

All testing was performed on a 7.0-T MRI scanner (Philips Achieva®, Philips Healthcare, Cleveland, OH) operating at 298 MHz. All medical implants underwent a series of tests in consecutive order including: (1) translational displacement, (2) rotational displacement, (3) image artefact production and (4) RF-related heating. If an implant was found to be "MR Unsafe" for a specific test, subsequent testing was not performed. 39 medical implants were gathered through a campus-wide network of physicians and researchers as well as through manufacturers, assigned a testing number and catalogued using their make, model, manufacturer, location in the body and material (as seen in Table 1). The implants included 26 orthopaedic implants, 8 vascular implants, 3 cranial implants and 2 ocular implants.

Translational attraction testing

The translational displacement forces were assessed for all 39 medical implants listed in Table 1. Since the force of the magnet correlates directly with the spatial gradient, the point at which the highest magnetic gradient occurs poses the most potential hazard to patients. This area was located by mapping the static magnetic field using a vector magnetometer (model THM-1176; Metrolab Technology, Geneva, Switzerland) and measuring the magnetic strength at 5-cm increments starting at the isocentre of the magnet.

The translational displacement test as described by the ASTM standard F2052-06[26] was performed on each implant at the location of the highest accessible spatial gradient. The implants were tied to a 20-cm string (<1% the mass of each implant) that was placed at the centre of an apparatus to which a protractor

Table 1. Biomedical implants tested for magnetic field interactions at 7.0 T

Item number	Manufacturer	Description	Implant type	Material(s)
1	Cook Medical Bloomington, IN	Zenith Flex® AAA Endovascular Graft Bifurcated Main Body Graft G48409	Vascular	Polyester fabric sewn to stainless steel
2	Cook Medical Bloomington, IN	Zenith TX2® TAA Endovascular Graft with Pro-Form G53422	Vascular	Polyester fabric sewn to stainless steel
3	Cook Medical Bloomington, IN	Zenith Flex® AAA Endovascular Graft Bifurcated Main Body Graft G48406	Vascular	Polyester fabric sewn to stainless steel
4	Cook Medical Bloomington, IN	Zenith TX2® TAA Endovascular Graft with Pro-Form G53418	Vascular	Polyester fabric sewn to stainless steel
5	Cook Medical Bloomington, IN	Zenith TX2® TAA Endovascular Graft with Pro-Form G53433	Vascular	Polyester fabric sewn to stainless steel
6	Cook Medical Bloomington, IN	GORE PROPATEN® Vascular Graft	Vascular	Polyester fabric sewn to stainless steel
7	Cook Medical Bloomington, IN	G2 Vena Cava Filter G21360	Vascular	Conichrome
8	Cook Medical Bloomington, IN	Filter inserted into stent	Vascular	Stainless steel
9	Alcon Fort Worth, TX	IQ Toric Intraocular Lens	Ocular	Acrylate/methacrylate copolymer
10	Alcon Fort Worth, TX	Intraocular Convexoplano Optic Lens	Ocular	Polymethylmethacrylate
11	DePuy Synthes Orthopaedics Warsaw, IN	Titanium Femoral Solid Nails 467.36	Femur	Titanium
12	DePuy Synthes Orthopaedics Warsaw, IN	Locking Calcaneal Plate short, right 241.622	Calcaneus	Stainless steel
13	DePuy Synthes Orthopaedics Warsaw, IN	4.5 mm Broad LCP Plates 226.621	Fractured bone	Stainless steel
14	DePuy Synthes Orthopaedics Warsaw, IN	4.5 mm Narrow LCP Plates 224.621	Fractured bone	Stainless steel
15	DePuy Synthes Orthopaedics Warsaw, IN	Proximal Tibia Less Invasive Stabilization System 422.304	Tibia	Titanium
16	DePuy Synthes Orthopaedics Warsaw, IN	2.7 mm LCP Distal Fibula Plate System 02.112.148	Fibula	Stainless steel
17	DePuy Synthes Orthopaedics Warsaw, IN	3.5 mm Wide Angle, Straight Reconstruction Plate 02.100.215	Pelvis	Stainless steel
18	DePuy Synthes Orthopaedics Warsaw, IN	Proximal Femur Plate 242.112	Femur	Titanium
19	DePuy Synthes Orthopaedics Warsaw, IN	3.5 mm LC-DCP Plate 223.6	Pelvis	Stainless steel
20	DePuy Synthes Orthopaedics Warsaw, IN	LCP Medial Distal Tibial Plates (right) 239.912	Calf	Stainless steel
21	DePuy Synthes Orthopaedics Warsaw, IN	LCP Medial Distal Tibia Plates 85-mm Screw	Orthopaedic	Titanium
22	DePuy Synthes Orthopaedics Warsaw, IN	65 mm Screw for LCP Fibula Plate System 422.395	Orthopaedic	Titanium
23	Zimmer Warsaw, IN	Zimmer NexGen LPS-Flex Mobile Bearing Knee 00-5764-015-51	Knee joint	Stainless steel

(Continued)

Table 1. (Continued)

Item number	Manufacturer	Description	Implant type	Material(s)
24	Zimmer Warsaw, IN	Zimmer NexGen LPS-Flex Mobile Bearing Knee (pre-coated stemmed plate)	Knee joint	Cobalt chrome alloy
25	Zimmer Warsaw, IN	Grade 5 titanium alloy	Hip and femur	Ti6Al4V titanium alloy
26	Zimmer Warsaw, IN	Extension for femoral head coverings to ball and socket joint (Implants 30 and 31)	Hip and femur	Ti6Al4V Titanium alloy
27	Zimmer Warsaw, IN	BIOLOX® OPTION Ceramic Femoral Head System 12/14	Hip and femur	Aluminium oxide matrix composite ceramic
28	Zimmer Warsaw, IN	Femoral head covering ball attached to hip implant (Implant 30) to form ball and socket joint	Hip and femur	Aluminium oxide matrix composite ceramic
29	Henry Schein Melville, NY	Single Tooth Bridge Restoration Camlog Screw	Maxillary /mandibular bone	Titanium
30	KLS Martin Jacksonville, FL	Burr Hole, Lot 32569770	Skull	Titanium
31	GPC Medical Ltd Vikaspuri, New Delhi	Orbital Plate with Bridge 818.156	Skull	Titanium
32	GPC Medical Ltd Vikaspuri, New Delhi	Mini Plate with Bridge 817.156	Skull	Titanium
33	DePuy Synthes Orthopaedics Warsaw, IN	S-ROM (Femoral Stem) Revision Hip Solutions	Hip and femur	Titanium with hydroxyapatite
34	Convidien	Monofilament Steel 3151 Non-absorbable Suture	Sternum	Stainless steel
35	Stryker	Gamma3 Locking Nail (Long Section) 1822-1242	Hip	Titanium alloy with Type II anodization (Ti-6Al-4v)
36	Stryker	Gamma3 Locking Nail (Short Screw Section) 3125-1180X	Hip	Titanium alloy with Type II anodization (Ti-6Al-4v)
37	Stryker	Omnifit Cemented Head/Neck* Long Stem Implants 6080-0530-200L	Hip	Cobalt chromium alloy
38	Stryker	Distal Medial Tibial Plate Model W20576 and 437228	Tibia	Stainless steel
39	Stryker	Dall-Miles Trochanter Cable Grip System 14841701	Hip	VITALLIUM—Cobalt, chromium and molybdenum

was attached in order to measure the deflection angle caused by the pull of MRI. At a displacement angle of 45°, the force of gravity is equal to the translational force of the magnet; therefore, if the magnet exerted more force on an object than gravity, *i.e.* the measured deflection angle exceeds 45°, the object fails the translational test. Each implant was tested for displacement angles three times, and the resulting angles were averaged. Those implants with a mean deflection angle $>45°$ were classified as "MR Unsafe" for this 7.0-T MRI environment. Implants with a mean deflection angle $\leq 45°$ progressed to the qualitative test for rotational displacement.

Qualitative torque test

To qualify the rotational displacement resulting from torque, the speed at which the implant rotated and aligned with the magnetic field was directly observed and rated at the isocentre. Qualifying implants were subjected to rotational displacement testing using adapted methodologies approved by the ASTM Standard F2213-06.[27] Implants were placed at the isocentre and on an apparatus marked with a gridded circle, segmented every 45° (Figure 1).

Each test object was directly observed for any type of possible movement with respect to alignment or rotation to the magnetic field. The investigator observed the torque test from within the magnet bore. The test object was moved 45° relative to its previous position and again observed for alignment or rotation to encompass a full 360° rotation of positions for each implant or device. Based on the speed of alignment, the implants were then qualitatively ranked on a scale of 0–4.[28] The following qualitative scale was used to describe alignment or rotation; 0,

Figure 1. A schematic of the apparatus used to test the rotational displacement of the implants. The black rectangle represents the implant. This apparatus consisted of a gridded circle with every 45° increment for the entire 360° of the circle marked.

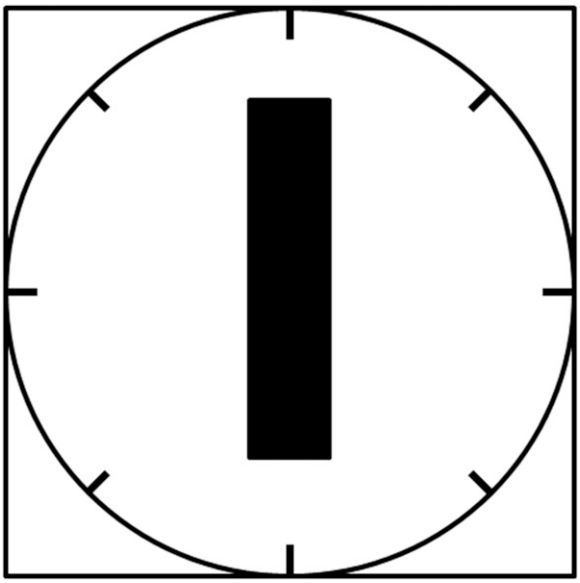

no torque; +1, mild or low torque, the device slightly changed its orientation but did not align to the magnetic field; +2, moderate torque, the device aligned gradually to the magnetic field; +3, strong torque, the device showed rapid and forceful alignment to the magnetic field; +4, very strong torque, the device showed very rapid and very forceful alignment to the magnetic field. The highest qualitative torque values are reported. This procedure was repeated three times for each implant tested, and the mean value was calculated. Implants evaluated between 0 and 2 were deemed safe for further analysis. Implants that received a rating of 3–4 were marked as "MR Unsafe" and were not evaluated for image artefacts or RF heating.

Image artefact testing

All implants receiving a status of "MR Conditional" in the translational and rotational tests were included in the image artefact testing according to the ASTM Standard F2119-07.[29] The implants were suspended within a phantom comprised of a solution of copper sulfate.[5] The aqueous copper sulfate solution had a concentration of 1.5 $g\,l^{-1}$ and was used to shorten the T_1 relaxation time with negligible effects on signal reception.

The phantom was then placed in the transmit/receive head RF coil (Nova Medical Inc., Wilmington, MA) and placed at the isocentre of the 7.0-T MRI scanner. MRI images for each implant were gathered using gradient-echo sequences (repetition time/echo time (TR/TE) = 166 ms/3.5 ms; field of view (FOV), $140 \times 160\,mm^2$; matrix, 72×70 pixels; 30 slices) with the imaging planes along the long axis of the implant. Data analysis was performed in MATLAB® (Mathworks®, Natick, MA) for the calculation of signal void area. The artefact volume was then manually delineated by three independent users and quantified by combining the areas of each image slice and producing a voxel value given in cubic millimeters along with the maximum area affected given in square millimeters. The mean calculated volume is reported.

Radiofrequency-induced heating testing

This experiment examined each implants' heat absorption capacity. When implants absorb excessive thermal energy (as is the case when imaging using RF pulses), the heat is able to dissipate into the surrounding tissue, which, if significant, can cause damage. Eight implants that represented a wide range of implant locations across the body were chosen for RF heating assessment. The ASTM Standard F2182-11a was used as a guide for these procedures.[30] Saline gel was created to mimic the conductivity of the human body using NaCl of concentration 2.92 $g\,l^{-1}$ and poly acrylic acid of concentration 20 $g\,l^{-1}$. The solution had a conductivity of 0.47 $S\,m^{-1} \pm 10\%$. Each implant tested was suspended in the gel solution in the location of the highest background local specific absorption rate (SAR) as determined experimentally. Four fibre optic temperature probes (model FOT-M; Fiso Technologies Inc, Quebec, Canada) were arranged around the implant in locations presumed to have the highest energy deposition, *i.e.* the tips of elongated devices.[23] The implant and temperature probes were suspended in the solution and placed in the transmit/receive head coil.

MR-related temperature changes were continuously measured using fluoroptic thermometry prior to (300 s) and during application of a pulse sequence designed to create extreme MRI-related heating conditions. Thus, an RF-intensive spin-echo sequence was implemented with a TR of 681 ms, initial TE of 6.8 ms and flip angle of 90°. An imaging matrix of 80×80 pixels was used with FOV equal to 240 mm^2 with 15 dynamic scans performed, resulting in a total imaging time of 14 min, 41 s. To elicit maximum SAR, a fat saturation band was placed over the volume of interest with a 60-mm thickness transmitted at 4 μT. The positions of the thermometry probes were inspected and verified immediately before and after the MRI-related heating experiment. The highest temperature rises are reported, herein.

RESULTS

Table 2 summarizes the findings for the deflection angles, torque values, measured image artefacts and RF heating for the 39 implants. In general, the test results for one test were not indicative of those for another, *i.e.* those implants that exhibited a large deflection angle were not necessarily experiencing a strong torque or producing larger image artefacts. The Zimmer NexGen® LPS-Flex Knee Joint (Warsaw, IN) comprised of stainless steel demonstrated the most magnetic field interactions with a deflection angle of 16°, a mild torque and the largest measured image artefacts.

Translational attraction

The largest patient-accessible spatial gradient (720 $G\,cm^{-1}$) was found to be located 145 cm from the isocentre at the external boundary of the magnet housing, and this point was used for translational displacement testing (Figure 2). 39 implants were tested with results shown in Table 2. 34 implants were classified as "MR Conditional" based on the translational test. Two of the endovascular grafts (Implants 1 and 4), a calcaneal plate (Implant 12)

Table 2. Summary of testing results

Implant	Deflection angle (°)	Torque value	Average artefact volume (mm^3)	Largest artefact area (mm^2)	Temperature change (°C)
1	90	N/A	N/A	N/A	N/A
2	2	0	152,090	5366	N/A
3	0	0	52,168	2509	0.14
4	90	N/A	N/A	N/A	N/A
5	3	0	129,280	4437	N/A
6	1	0	6021	634	N/A
7	5	0	4155	549	N/A
8	5	0	25,551	1022	−0.16
9	0	0	0	0	N/A
10	0	0	0	0	N/A
11	1	0	N/A	N/A	N/A
12	46	N/A	N/A	N/A	N/A
13	44	N/A	482,279	10,280	N/A
14	44	N/A	352,186	10,231	N/A
15	4	0	93,582	3976	N/A
16	36	0	105,319	3573	0.41
17	43	0	198,764	8256	N/A
18	44	0	N/A	N/A	N/A
19	45	0	129,320	4243	−0.54
20	42	0	371,082	10,287	N/A
21	3	0	19,010	746	N/A
22	4	0	14,890	5531	0.21
23	16	1	1,000,477	11,362	N/A
24	5	0	173,226	5694	N/A
25	5	1	N/A	N/A	N/A
26	4	0	202,937	3613	N/A
27	0	0	61,979	3178	N/A
28	17	0	392,328	6137	N/A
29	7	0	5990	347	0.20
30	7	2	3430	191	−0.07
31	7	0	2488	268	N/A
32	6	0	5983	476	N/A
33	4	1	N/A	N/A	N/A
34	32	0	N/A	N/A	−0.17
35	0	0	N/A	N/A	N/A
36	7	0	N/A	N/A	N/A
37	15	0	N/A	N/A	N/A
38	47	N/A	N/A	N/A	N/A
39	18	0	N/A	N/A	N/A

For evaluation in the 7.0-T MRI environment, medical implants underwent a series of tests including (1) translational displacement, (2) rotational displacement, (3) image artefact production and (4) RF-related heating in the consecutive order.

Figure 2. The static magnetic field strength gradient as a function of distance from the isocentre of the magnet. The largest spatial gradient is located 135 cm from the isocentre of the 7-T MRI scanner.

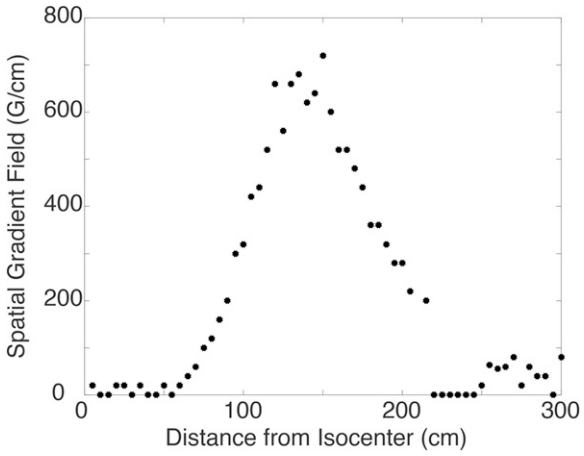

and a tibial plate (Implant 38) (as named in Table 1) had average deflection angles above the ASTM mandated 45° and were automatically classified as "MR Unsafe" and underwent no further testing. It is important to note that various orthopaedic plates (Implants 13, 14, 18 and 19) had average deflection angles near or equal to 45°.

Qualitative assessment of torque

33 implants underwent the rotational testing. Two implants that were determined to be "MR Conditional" in the deflection angle test were excluded from the rotational testing owing to large deflection angle measurements including Implant 13 (4.5 mm Synthes Broad LCP Plates, Warsaw, IN) and Implant 14 (4.5 mm Synthes Narrow LCP Plates). The results of the qualitative assessment of torque (shown in Table 2) ranged from 0, no torque, to 2, moderate torque—the test object aligned gradually to the magnetic field. The highest value recorded, moderate torque, only occurred with the Burr Hole manufactured by KLS Martin (Implant 30 from Table 1), while the other 32 implants had values of either no torque or mild torque.

Image artefact testing

The artefact testing included 26 implants with measured artefact volumes ranging from 0 to 1,000,477 mm^3, which was produced by the Zimmer NexGen LPS-Flex Mobile Bearing Knee (Implant 23 in Tables 1 and 2). Image artefact areas ranged from 0 to 11,362 mm^2 with the largest area within one slice affected, also created by the Zimmer NexGen LPS-Flex Mobile Bearing Knee. In order to appreciate average artefact sizes, example image artefact data for the Cook Medical Endovascular Graft with ProForm Model G53422 (Implant 2) and the Zimmer Hip Implant (Implant 28) are shown in Figure 3a and Figure 3b, respectively. The resulting image artefacts are shown below in panels Figure 3c and Figure 3d, respectively. When comparing panels Figure 3c and Figure 3d, the different manifestations of signal loss are apparent, further supporting the need for comprehensive safety testing implants prior to routine use.

Radiofrequency-induced heating testing

RF heating tests were performed in a select subset of eight implants and resulted in only a slight increase in temperature with results found in Table 2 and Figure 4. Only Implants 16, 22 and 29 demonstrated an increase in temperature as a result of the applied RF pulses (Figure 4a–c), with the highest temperature rise being 0.41 °C arising from the 2.7-mm LCP Distal Fibula Plate System manufactured by DePuy Synthes (Implant 16). Implants 19, 30, 34 and 8 did not display an increase in temperature for the duration of the examination (Figure 4e–h), while Implant 3 demonstrated a slight increase in temperature

Figure 3. The implant size/shape relative to the artefact in scale. Panels (a) and (b) show photographs of Implants 2 and 28, respectively, while panels (c) and (d) display example MRI data used to measure artefact area and volume.

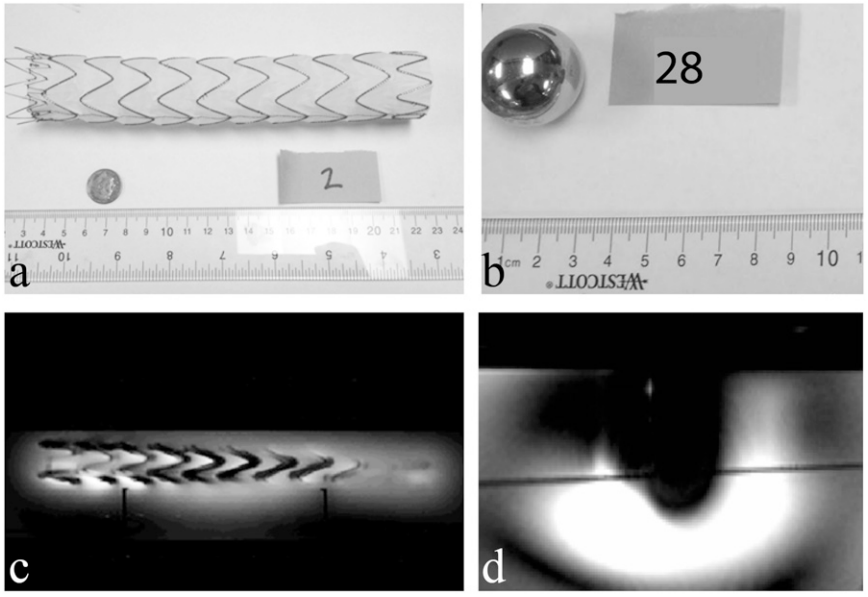

(Figure 4d). The greatest increase in temperature recorded was 0.41 °C over the 30 min observed, which was found for the Synthes 2.7-mm LCP distal fibular plate system (Implant 16). Implants 19, 33 and 45 exhibited decreased temperature measurements throughout the MR procedures.

DISCUSSION

MRI at 7.0 T allows for higher resolution imaging, but owing to the current lack of implant testing done to ensure participant safety in a 7.0-T MRI environment, the applicable population is limited. This study expands the growing safety database of rated implants at 7.0 T.[22–25] Of the 39 medical implants tested, the 4 implants that failed included 2 stents, 1 heel implant and 1 fibular implant. All four of these implants failed during the translational testing as they were immediately reactive to the field. All other safety tests conducted on the remaining implants did not result in any implant failing, meaning no implant had a deflection angle >45°, a greater than moderate torque or a temperature change >1 C.

Image artefact testing quantifies the distortion of the images caused by the interaction between the implant and the magnetic field manifesting as a signal void in the images. Artefacts do not cause physical harm to the patient, although it is important to note that a patient screened with one of the designated implants would have an area of distortion near the implant that could limit image accuracy in that area. For example, the burr hole cover reviewed in this study (Implant 30 manufactured by KLS Martin) has the potential to mask an abnormality in the brain. The largest single-slice signal dropout observed was approximately 11,362 mm^2, while the largest signal void volume created by an implant was 1,000,477 mm^3, produced by the Zimmer NexGen LPS-Flex Mobile Bearing Knee.

During an MRI scan, the pulsed RF field induces currents in the human body causing tissue heating. The presence of an electrically conducting medical implant will concentrate these RF-induced currents potentially causing additional tissue heating and posing danger to the subject. In particular, the probability of elongated objects coupling with the RF electric field of the scanner increases with heightened static magnetic field strengths. High local RF-induced voltages at the tips of these objects can cause a localized increase of power deposition, proportional to the square of the electric field strength. Furthermore, according to Faraday's law, the induced voltages in the implant increase with the increase in Larmor frequency (proportional to the static magnetic field) and hence are also a consideration for 7.0-T MRI examinations. It is important to note that the orientation of the implant will influence the locally focused electric fields and therefore determine the extent of heating.

RF heating test results showed minimal change in the temperature of the implants tested, with the change in temperature ranging from −0.5 to 0.41 C, although these results are specific to the implant location, orientation and coil. Three of the tested implants exhibited a decrease in temperature during the RF heating tests. These temperature decreases near the surface of the implants could be due to a number of variables. It is possible that the implants were not placed at the location of the highest RF deposition, which could have been specifically determined with more detailed information from the coil manufacturer and

Figure 4. Changes in temperature over time from radiofrequency-induced heating on selected medical implants. Panels (a–c) display those implants that increased in temperature. Panel (d) shows the time course of Implant 3 which did not change in temperature and panels (e–h) display those implants that had decreasing temperature during the observed time.

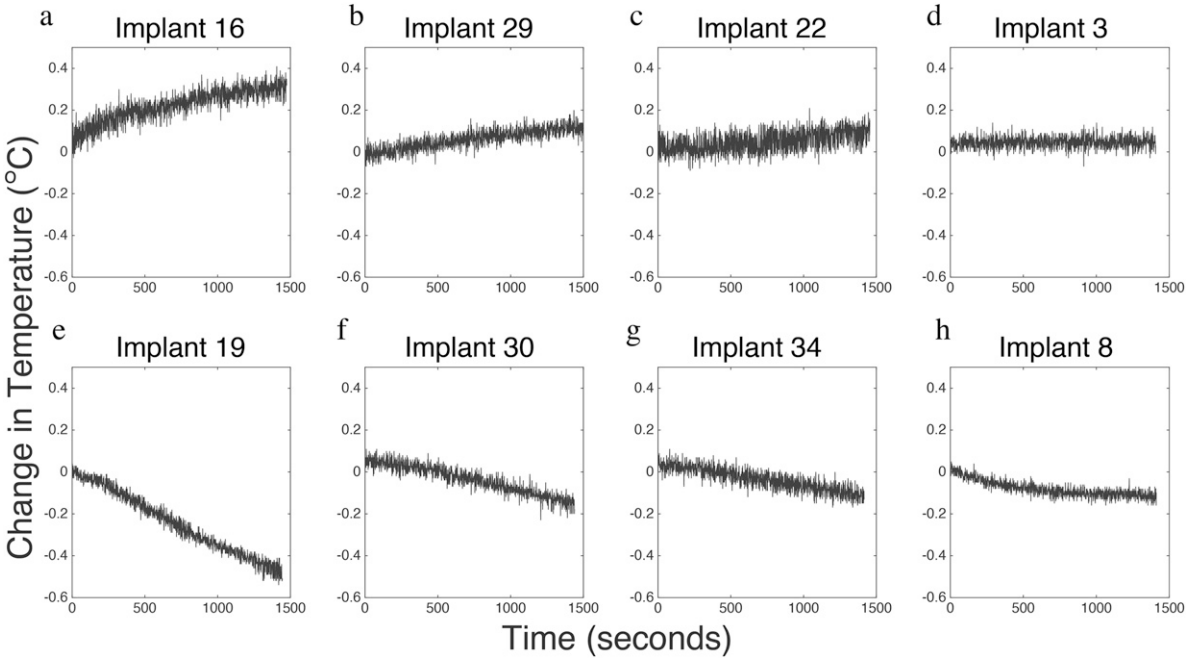

subsequent numerical simulations of the RF field pattern. It is also possible that these implants did not reach temperature equilibrium prior to the start of the RF heating experiment, in which case the recorded decrease in temperature would be a result of the phantom/implant adjusting to the ambient temperature in the scan environment. With the development of body part-specific coils, further research is necessary to ensure that this minimal change in temperature is valid for the implant in its corresponding coil (*e.g.* testing a knee implant in a leg-specific coil). Although with the SAR set to 212% to cause the "worst case scenario" in which an implant would be exposed to the greatest increase in temperature, differences in temperature change between the coils may be nominal.

Four implants showed signs of potentially dangerous interactions with the 7.0-T MRI environment, although, by the ASTM standards they would not be classified as "MR Unsafe". A few of the orthopaedic implants manufactured by Synthes, specifically Implants 13, 14, 18 and 19, had average deflection angles slightly $\leq$45°, which is still considered safe by the ASTM standard,[26] but should be carefully considered prior to placement in the 7.0-T MRI environment. Overall, Implants 2, 3, 8, 16, 19, 29, 30 and 34 can be marked as "MR Conditional" for this 7.0-T MRI environment.

Despite having similar manufacturers, functions, models and structures, some implants had drastically different results. The implants tested were primarily composed of either titanium or stainless steel, as listed by the supplier. The composition of the implants had an influence on the outcomes of the safety testing. In the case of Cook Medical's endovascular grafts (Implants 1, 2, 3 and 4), even though all came from the same manufacturer who listed them as produced from the same material with comparable structure, the deflection angle assessment produced very different outcomes. This may have been due to the different grades of steel involved in production. Accurate information in regards to model number and version is essential to ensure that the exact composition of the implants is known, and care must be taken when generalizing results.

It is important to highlight the contrasting results of specific implants when tested at varying field strengths. For example, all coronary artery stents chosen for this study were rated at most "MR Conditional" at 1.5 and 3.0 T strengths,[17] but two of these stents (Implants 1 and 4) displayed deflection angles of 90° before even reaching the location of the largest gradient and hence were classified as "MR Unsafe" for the 7.0-T MRI environment. Orthopaedic implants followed this same pattern, where all implants tested at 1.5 and 3.0 T were at most "MR Conditional", but two orthopaedic implants tested in this study had average deflection angles of >45°.

The implants assessed for safety in the 7.0-T MRI environment for this study represent only a small sample. The majority of research conducted using 7.0-T MRI focuses on the brain and upper regions of the body; therefore, the presented RF heating and image artefact assessments were limited to the standard head coil. However, with the development of imaging coils for other areas of the body, the focus of research may shift in the future and encompass other anatomies. Accordingly, future work will expand on implant location and available coils. Situation-specific assessment is necessary to ensure safety in regards to RF heating for the implants tested as the degree of energy absorbed and dissipated are sample, coil and sequence specific.

CONCLUSION

This study presents a total of 39 common biomedical implants tested for magnetic field interactions in the 7.0-T MRI environment. All 39 implants were tested for translational displacement with 4 exhibiting substantial magnetic field interactions, with all 4 implant types considered at least conditional if not safe in a 3.0-T MRI environment. Of the 33 implants tested for rotational displacement, only 1 exhibited moderate torque. RF heating effects for the eight implants tested showed no significant increases in temperature. Of the implants tested, only Implant 19 (Limited Contact Dynamic Compression Plate for the Pelvis, 3.5 mm, manufactured by Synthes) has shown signs of being potentially hazardous in a 7.0-T MRI environment owing to its high but still allowed deflection angle and therefore could be labelled as "MR Conditional". Three other implants demonstrated signs of conditionally passing, but complete testing needs to be conducted before proper labelling occurs. All results gathered in this study and future medical implant safety studies are vital in ensuring the safety of potential research participants for studies using the 7.0-T MRI and are helping to further the expansion of the biomedical implant safety database in the 7.0 T MRI environment. Medical implant safety testing at 7.0 T is an imperative conduit for more in-depth extensive research on pathologies such as cancer, multiple sclerosis, Parkinson's disease and many others. Recently, an FDA-approved 7.0- T MRI scanner was announced. Clinical use of this field strength will foster the growth of research, hence increasing availability and further justifying safety studies such as that presented herein.

FUNDING

This research is supported by The National Institutes of Health, NCATS 5KL2 RR024977 (AND), the American Society of Radiologic Technologist (ASRT) Foundation Grant ASRT F13_RG_003 Research Grant (AND and DRP) and School for Science and Math at Vanderbilt (SSMV) and the Center for Science Outreach (DXF, JPM, FKM, RAS and MEL).

ACKNOWLEDGMENTS

Special thanks to Amanda Dixon, Dr Josh Brogan and Dr Stephanie Weeden-Wright for their time and effort on this project.

REFERENCES

1. van der Kolk AG, Hendrikse J, Zwanenburg JJ, Visser F, Luijten PR. Clinical applications of 7 T MRI in the brain. *Eur J Radiol* 2013; **82**: 708–18. doi: 10.1016/j.ejrad.2011.07.007
2. Duchin Y, Abosch A, Yacoub E, Sapiro G, Harel N. Feasibility of using ultra-high field (7 T) MRI for clinical surgical targeting. *PloS One* 2012; **7**: e37328. doi: 10.1371/journal.pone.0037328
3. De Ciantis A, Barkovich AJ, Cosottini M, Barba C, Montanaro D, Costagli M, et al. Ultra-high-field MR imaging in polymicrogyria and epilepsy. *AJNR Am J Neuroradiol* 2015; **36**: 309–16. doi: 10.3174/ajnr.A4116
4. Pan JW, Duckrow RB, Gerrard J, Ong C, Hirsch LJ, Resor SR Jr, et al. 7T MR spectroscopic imaging in the localization of surgical epilepsy. *Epilepsia* 2013; **54**: 1668–78. doi: 10.1111/epi.12322
5. Jones CK, Huang A, Xu J, Edden RA, Schär M, Hua J, et al. Nuclear overhauser enhancement (NOE) imaging in the human brain at 7T. *NeuroImage* 2013; **77**: 114–24. doi: 10.1016/j.neuroimage.2013.03.047
6. Paech D, Zaiss M, Meissner JE, Windschuh J, Wiestler B, Bachert P, et al. Nuclear overhauser enhancement mediated chemical exchange saturation transfer imaging at 7 Tesla in glioblastoma patients. *PloS One* 2014; **9**: e104181. doi: 10.1371/journal.pone.0104181
7. Wattjes MP, Barkhof F. High field MRI in the diagnosis of multiple sclerosis: high field-high yield? *Neuroradiology* 2009; **51**: 279–92. doi: 10.1007/s00234-009-0512-0
8. Tallantyre EC, Morgan PS, Dixon JE, Al-Radaideh A, Brookes MJ, Evangelou N, et al. A comparison of 3T and 7T in the detection of small parenchymal veins within MS lesions. *Invest Radiol* 2009; **44**: 491–4. doi: 10.1097/RLI.0b013e3181b4c144
9. Dula AN, Smith SA, Gore JC. Application of chemical exchange saturation transfer (CEST) MRI for endogenous contrast at 7 Tesla. *J Neuroimaging* 2013; **23**: 526–32. doi: 10.1111/j.1552-6569.2012.00751.x
10. Nakada T, Matsuzawa H, Igarashi H, Fujii Y, Kwee IL. *In vivo* visualization of senile-plaque-like pathology in Alzheimer's disease patients by MR microscopy on a 7T system. *J Neuroimaging* 2008; **8**: 125–9. doi: 10.1111/j.1552-6569.2007.00179.x
11. Kerchner GA. Ultra-high field 7T MRI: a new tool for studying Alzheimer's disease. *J Alzheimers Dis* 2011; **26** (Suppl. 3): 91–5. doi: 10.3233/JAD-2011-0023
12. Benjamin P, Viessmann O, MacKinnon AD, Jezzard P, Markus HS. 7 Tesla MRI in cerebral small vessel disease. *Int J Stroke* 2015; **10**: 659–64. doi: 10.1111/ijs.12490
13. Kwon DH, Kim JM, Oh SH, Jeong HJ, Park SY, Oh ES, et al. Seven-Tesla magnetic resonance images of the substantia nigra in Parkinson disease. *Ann Neurol* 2012; **71**: 267–77. doi: 10.1002/ana.22592
14. Shellock FG, Kanal E, Gilk TB. Regarding the value reported for the term "spatial gradient magnetic field" and how this information is applied to labeling of medical implants and devices. *AJR Am J Roentgenol* 2011; **196**: 142–5. doi: 10.2214/AJR.10.5004
15. Shellock FG, Crues JV. MR procedures: biologic effects, safety, and patient care. *Radiology* 2004; **232**: 635–52. doi: 10.1148/radiol.2323030830
16. Hargreaves BA, Worters PW, Pauly KB, Pauly JM, Koch KM, Gold GE. Metal-induced artifacts in MRI. *AJR Am J Roentgenol* 2011; **197**: 547–55. doi: 10.2214/AJR.11.7364
17. Shellock FG. The list. 2015. Available from: www.mrisafety.com/The List_search.asp
18. Woods TO. Standards for medical devices in MRI: present and future. *J Magn Reson Imaging* 2007; **26**: 1186–9. doi: 10.1002/jmri.21140
19. Kanal E, Froelich J, Barkovich AJ, Borgstede J, Bradley W Jr, Gimbel JR, et al; American College of Radiology Subcommittee on MR Safety. Standardized MR terminology and reporting of implants and devices as recommended by the American College of Radiology Subcommittee on MR Safety. *Radiology* 2015; **274**: 866–70. doi: 10.1148/radiol.14141645
20. ASTM. *Standard Practice for marking medical devices and other items for safety in the magnetic resonance environment*. West Conshohocken, PA: ASTM International; 2013.
21. Shellock FG, Woods TO, Crues JV 3rd. MR labeling information for implants and devices: explanation of terminology. *Radiology* 2009; **253**: 26–30. doi: 10.1148/radiol.2531091030
22. Thelen A, Bauknecht HC, Asbach P, Schrom T. Behavior of metal implants used in ENT surgery in 7 Tesla magnetic resonance imaging. *Eur Arch Otorhinolaryngol* 2006; **263**: 900–5.
23. Dula AN, Virostko J, Shellock FG. Assessment of MRI issues at 7 T for 28 implants and other objects. *AJR Am J Roentgenol* 2014; **202**: 401–5. doi: 10.2214/AJR.13.10777
24. Sammet CL, Yang X, Wassenaar PA, Bourekas EC, Yuh BA, Shellock F, et al. RF-related heating assessment of extracranial neurosurgical implants at 7T. *Magn Reson Imaging* 2013; **31**: 1029–34. doi: 10.1016/j.mri.2012.10.025
25. Schrom T, Thelen A, Asbach P, Bauknecht HC. Effect of 7.0 Tesla MRI on upper eyelid implants. *Ophthal Plast Reconstr Surg* 2006; **22**: 480–2. doi: 10.1097/01.iop.0000240807.42320.d9
26. ASTM. *Standard test method for measurement of magnetically induced displacement force on medical devices in the magnetic resonance environment*. West Conshohocken, PA: ASTM International; 2006.
27. ASTM. *Standard test method for measurement of magnetically induced torque on medical devices in the magnetic resonance environment*. West Conshohocken, PA: ASTM International; 2011.
28. Shellock FG. Biomedical implants and devices: assessment of magnetic field interactions with a 3.0-Tesla MR system. *J Magn Reson Imaging* 2002; **16**: 721–32. doi: 10.1002/jmri.10207
29. ASTM. *Standard test method for evaluation of MR image artifacts for passive implants*. West Conshohocken, PA: ASTM International; 2012.
30. ASTM. *Standard test method for measurement of radio frequency induced heating on or near passive implants during magnetic resonance imaging*. West Conshohocken, PA: ASTM International; 2012.